Quantitative assessment of the impact of second phase particle arrangement on damage and fracture anisotropy

F. Hannard, A. Simar, E. Maire, T. Pardoen

Quantitative assessment of the impact of second phase particle arrangement on damage and fracture anisotropy

F. Hannard[a], A. Simar[a], E. Maire[b], T. Pardoen[a]

[a] *Institute of Mechanics, Materials and Civil Engineering, Université catholique de Louvain, B-1348 Louvain-la-Neuve, Belgium*
[b] *MATEIS UMR5510, INSA-Lyon, F-69621 Villeurbanne, France*

Abstract

The fracture anisotropy of the three aluminium alloys Al 6056, Al 6061 and Al 6005A has been characterized in tension. In the three alloys, the onset of yielding and strain hardening behaviour do not significantly depend on the loading direction. However, while the fracture strain is close to isotropic in the alloys Al 6061 and Al 6005A, the alloy Al 6056 exhibits a clear fracture anisotropy. In situ tensile tests in X-ray tomography reveal that there exist two coalescence stages that include intra- and inter-cluster coalescence. A quantitative approach is proposed to relate the propensity to fracture anisotropy to a simple microscopic parameter characterizing the degree of anisotropy in the spatial distribution of second phase particles. The new indicator which quantifies the degree of connectivity or percolation between clusters is successfully assessed for the three Al alloys.

Keywords: X-ray tomography, Ductile damage, Anisotropy, Aluminium alloys

1. Introduction

Ductile fracture results from an overlapping sequence of nucleation, growth and coalescence of small internal cavities leading to macroscopic failure. The current state of understanding of the damage stages from a micromechanical viewpoint is relatively advanced and has allowed the development of predictive models well validated for sufficiently homogeneous materials <1>. Indeed, ductile damage has traditionally been treated as a global process, see for instance the enhanced version of the Gurson model <2; 3; 4; 5>, the material being often treated with ”average” microstructural properties assuming a strict progression from nucleation to coalescence. However, there are considerable experimental evidences which indicate that the ductile damage process is often strongly affected by microstructure heterogeneities.

The different types of microstructure heterogeneities which can influence the damage process have been thorougly reviewed in Ref. <6>. Heterogeneities can impact the damage process in two ways. First, coalescence might occur in some clustered regions or regions in which void nucleation was fast and void close to one another while other regions of the material do not exhibit any damage yet. Second, the anisotropy of the microstructure impacts the fracture behaviour and can induce significant anisotropy in the mechanical properties, which is at the core of the present work.

Three types of sources of anisotropy can impact the fracture behaviour :

1. *Plastic anisotropy* is related to the crystallographic texture as caused for instance by the preferred orientation of the grains along the rolling direction. The plastic flow anisotropy has indeed a significant influence on the ductile failure as void growth is driven by plastic deformation of the surrounding material <7; 8>.

2. *A morphological anisotropy* can originate both from the shape of the voids or from the shape of the particles at which voids nucleate with a preferential orientation of their main axis. For instance, void nucleation by particle cracking is dependent on the loading direction because particles preferentially aligned along the processing direction <9; 10> undergo larger load transfer <11>. For instance, Benzerga and Keralavarma used cell model analyses to show that the void aspect ratio significantly affects the overall ductility <12>.

3. *A topological anisotropy* can result from the spatial distribution of particles. It particularly affects the void coalescence step. During the forming process, brittle intermetallic particles are broken and a stringer-type particle clustering develop along the rolling direction. This source of anisotropy is further addressed in this study and a deeper coverage of the literature is provided in the next paragraphs.

The topological anisotropy of fracture properties has been increasingly characterized in recent years. One of the first analysis of the void spacing effect on the coalescence stage is due to Koplik<13> and then further commented in Ref. <4>. Lassance *et al*. <14> have used finite elements (FE) unit cell calculations to study the effect of void distribution on ductility. It was concluded that for a metal with a volume fraction of particles of 1%, the ductility might change by more than a factor of 2 if the void spacing varies by a factor 2 when comparing two orthogonal directions. Thomson *et al*. have shown that the orientation of a particle cluster with respect to the direction of loading significantly influences the failure strain <15>. This effect has been studied experimentally in a model (Al-Si) material specifically fabricated to accentuate

second-phase particle clustering <16>. The formability was indeed found to be reduced when the loading direction was perpendicular to the major axis of the particle stringers. The clustering of particles into bands has also been linked to the anisotropic ductility of Al-2024 rolled plates as it creates an easy percolating crack path perpendicular to the rolling direction <17>. The effect of the loading direction on the ductility of two commercial aluminium alloys (AA5182 and AA5754) was investigated in Ref.<18>. The lack of orientation effect on the ductility of the alloy AA5754 compared to alloy AA5182 was attributed to a lower propensity for large and oriented stringer-like clusters. Bouchard *et al* <19> observed a strong anisotropic fracture behaviour in a classical manganese steel grade, while the hardening behaviour did not depend much on the direction of loading. In situ X-ray tomography tensile tests revealed that the strong anisotropy was mainly related to the direct influence of the particular inclusion spatial distribution with very elongated and aligned MnS inclusions. An anisotropic void distribution also has a significant effect on the resistance to crack initiation <20>.

In what is probably the most advanced study to date of the anisotropy effects on ductile fracture by Benzerga *et al*.<21>, all three sources of anisotropic damage, i.e. plastic, morphological and topological anisotropy, were characterized and it was concluded that the effect of void spacing on the void coalescence is of primary importance to explain the orientation dependence of ductility. However, more experimental work is required to develop simple and quantitative microscopic indicators of particle clustering and of its degree of anisotropy. The limited attention that has been given to this major effect is probably related to the difficulty to quantitatively distinguish between the various sources of damage.

In our previous study <22>, the ductility of three industrial Al alloys has been investigated under a wide range of heat treatment conditions. These three alloys involve relatively similar composition and volume fraction of iron-rich intermetallic particles (around 1%). However, the size of the particles is very different with an average equivalent diameter equal to 1.3μm, 2.1μm, and 3.1μm for the Al 6005A, Al 6061 and Al 6056, respectively. Major differences among the fracture strains in the different alloys were observed which were shown to be primarily dictated by the effect of particle size distribution with the alloy exhibiting the smallest particles nucleating voids later and thus being the most ductile. In the present investigation, the anisotropy of ductility between the main forming direction and the transverse direction has been characterized for these three alloys. The purpose of the paper is to propose a quantitative approach to relate the propensity to fracture anisotropy with a simple microscopic parameter characterizing the degree

of anisotropy of the spatial distribution of second phase particles.

2. Experimental methods

2.1. Materials

The Al alloys were provided in the form of extruded plates (6005A alloy) or of cold rolled plates (6061 and 6056 alloys). The thickness of the plates is equal to 6 mm for the 6005A and 6056 alloys and 4.7 mm for the 6061 alloy. These three alloys all present Mg and Si as main alloying element. There composition are given in Ref. <22>. Heat treatments at 300°C for various durations ranging from 10 s to 20 days have been performed on each material initially in the T6 state. Cross-comparisons of the three alloys can thus be made at similar initial yield stress.

2.2. Macroscopic tensile tests

Uniaxial tensile tests are performed under displacement control at constant velocity (1 mm/min). The tensile specimens are cylindrical, 4 mm in diameter, and the initial gauge length is equal to 30 mm. Tensile specimens were extracted perpendicular and parallel to the processing direction. The initial yield stress and the true strain at necking are noted σ_0 and ϵ_u, respectively. The true fracture strain has been measured post-mortem on the broken specimens and is quantified by $\varepsilon_f = \ln\left(\frac{A_0}{A_f}\right)$, where A_0 and A_f are the initial and final cross-sectional area, respectively.

2.3. Microstructure characterization

The characterization of the intermetallic particle fields is carried out based on scanning electron microscopy (SEM) and synchrotron-based X-ray microtomography. After standard polishing, the intermetallic particles are characterized by SEM operated at 15 kV under electron backscattered mode. SEM images, taken at a magnification of 600x in the processing-transverse plane, are combined in order to determine the spatial distribution of particles over a statistically representative area ($\approx 1.25\text{mm}^2$).

X-ray microtomography experiments are performed at the TOMCAT beamline of the Swiss Light Source <23>. The observed region is a cube of 260 μm side length and isotropic voxel size of 325 x 325 x 325 nm^3,

see <22> for more details.

2.4. *In situ tensile testing coupled to X-ray microtomography*

In situ tensile tests coupled to X-ray microtomography (voxel size of 0.6 x 0.6 x 0.6 μm^3) have been performed for the Al 6056 in T4 temper ($\sigma_0 \approx 250$MPa) in order to further investigate the effect of the loading direction on the evolution of the damage process and to understand the role of microstructure on fracture anisotropy. These tests are also performed at the TOMCAT beamline of the Swiss Light Source <23>. A dedicated in-situ tensile testing machine described in Ref. <24> has been mounted on the rotation stage of the 3D tomography setup <25>. The mini smooth tensile specimens, with diameter of 1 mm, are deformed up to fracture while the tensile force F is recorded. The data acquisition is made at regular discrete deformation steps.

3. Results

3.1. *Mechanical properties*

Figure 1(a) shows the true stress-true strain curves until necking for the three alloys in the T6 state, loaded along the rolling (plain line) and transverse direction (dashed line). All three alloys exhibit weak plastic anisotropy. The true stress-true strain response of the Al 6056 in overaged condition (63 hours at 300°C performed on the T6 state) is also shown in order to prove that the plastic anisotropy remains weak with heat treatments. Figure 1(b, c, d) summarize the results extracted from the tensile tests for the three alloys, loaded along the rolling and transverse directions, as a function of the initial yield stress σ_0 (corresponding to the various heat treatments). For the same value of σ_0, the tensile strength σ_{max} is very similar in every case (Fig. 1(b)). Strain rate sensitivity is weak in the 6xxx serie aluminium alloys <26> and, in agreement with the Considère condition, the mean strain hardening exponent n is equal to the strain at necking ϵ_u. The necking strains follow the same "banana" shape trend for the three alloys when plotted as a function of the yield stress, independently of the loading direction (Fig. 1(c)). It can thus be concluded from these observations that the plastic yielding behaviour is close to isotropic for the three alloys, i.e. the hardening behaviour does not depend much on the loading direction.

However, the fracture strains are very different when comparing the three alloys (Fig. 1(*d*)) and this has already been shown, see Ref.<22>, to be primarily dictated by the effect of particle size distribution with the alloy exhibiting the smallest particles being the most ductile. Figure 1(*c*) also shows that while the fracture strain is very similar for both loading directions in the 6061 and 6005A Al alloys, the anisotropy is significant for the Al 6056. Indeed, in this alloy, the fracture strain in the rolling direction is larger compared to the transverse direction at identical yield strength, especially for heat treatments leading to high strength.

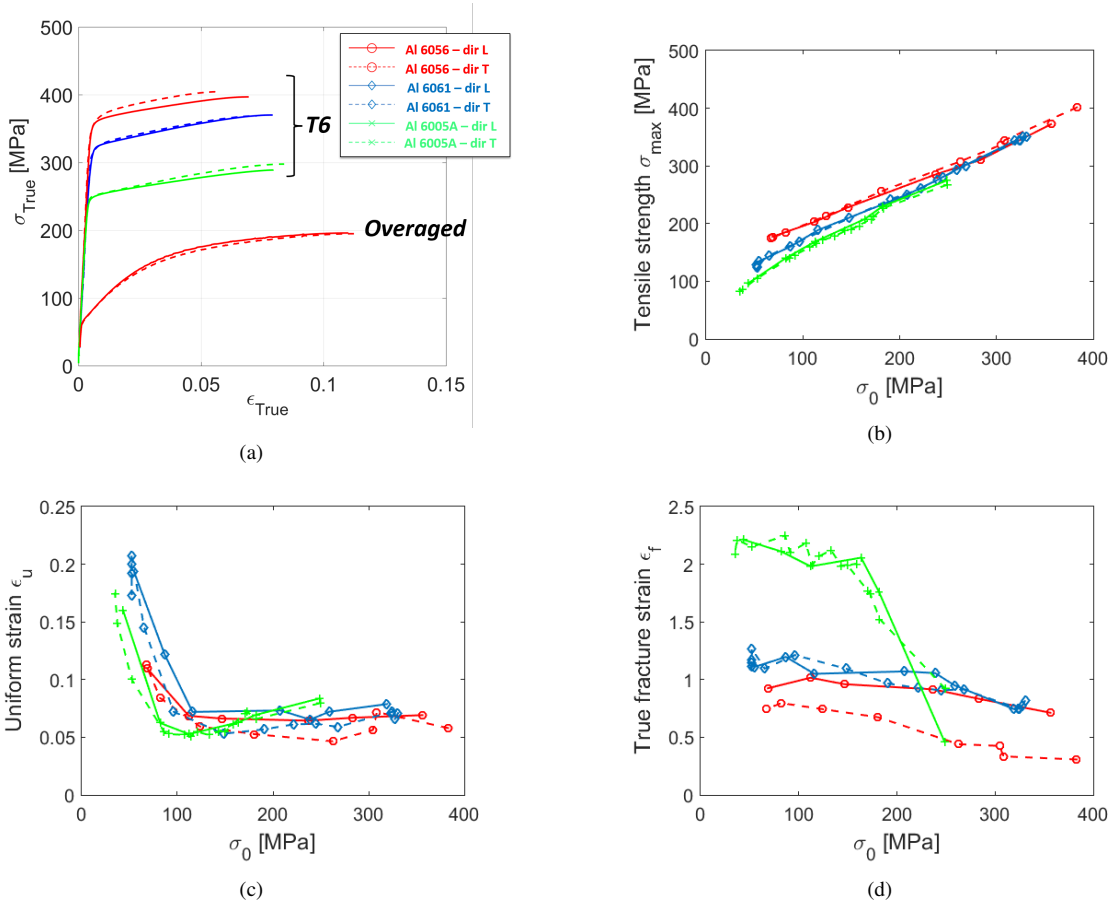

Figure 1: (*a*) True stress-true strain curves until necking for the three alloys in the T6 state and loaded along the rolling (plain line) and transverse direction (dashed line). Variation of the different parameters extracted from the uniaxial tensile tests on the three alloys as a function of the yield stress corresponding to the different heat treatments: (*b*) tensile strength of the three Al alloys; (*c*) true strain at the onset of necking; (*d*) true fracture strain.

3.2. Microstructure characteristics

Figure 2 shows part of the particle fields analysed using SEM images and Fig. 3 (left) shows a sub-volume extracted from the full tomographic volume for the three alloys. As expected, the particles are preferentially aligned along the processing direction, leading to stringer-type clustering. It seems that the clustering is more pronounced in the case of the Al 6056 but the quantification of the degree of clustering by visualization can be misleading as the size of the particles differs among the alloys. A rigorous method to quantify the degree of anisotropy of particle clustering is proposed in the following.

3.2.1. Quantification of the degree of microstructural anisotropy

The main question addressed here is whether the degree of anisotropy of particles clustering along the processing direction is large enough to affect the macroscopic ductility. In other words, the goal is to find a microstructural parameter which determines if the configuration of stringers can potentially lead to a percolating damage path perpendicular to the processing direction. The problem is physically related to the percolation of damage/microcracks over a length scale large enough to trigger the catastrophic failure of the specimen, hence it is necessary to quantify the long range characteristics of the particles spatial distribution. This means that more classical indicators based on the nearest neighbor analysis or Voronoi tesselation are not rich enough, as they focus on the short range characteristics of the particles neighbourhood. As a consequence, an extension in 2D and 3D of the radial distribution function (RDF) analysis is applied. In 1D, the RDF corresponds to the probability for a neighboring particle to be located at a distance r, in any direction <27>. The extended pair correlation function (PCF), in 2D and 3D, takes into account both the distance and angular dependence of the particles (preferentially aligned in one direction). **The PCF function is defined, in 3D, as the probability for a given point at position $\vec{r}$ to be located inside a particle, given that another particle is located at the origin of the reference system**. A PCF value smaller or larger than 1 corresponds, respectively, to a smaller or larger probability to find a neighbor in the vicinity of a particle compared to a perfectly homogeneous distribution. The PCF function accounts for both distance and angular dependence of the particles spacing. The effects of the particle size and shape are also naturally accounted for in the PCF function since it takes into account the full particle volumes and not only the position of the centroids. Indeed, all three alloys have a particle shape factor close to 2 with particles preferentially elongated along the processing direction (see <22> for more details). Furthermore, the size of the particles strongly differs when comparing the three alloys, as already explained and shown in Figures 2 and 3. The PCF function is thus

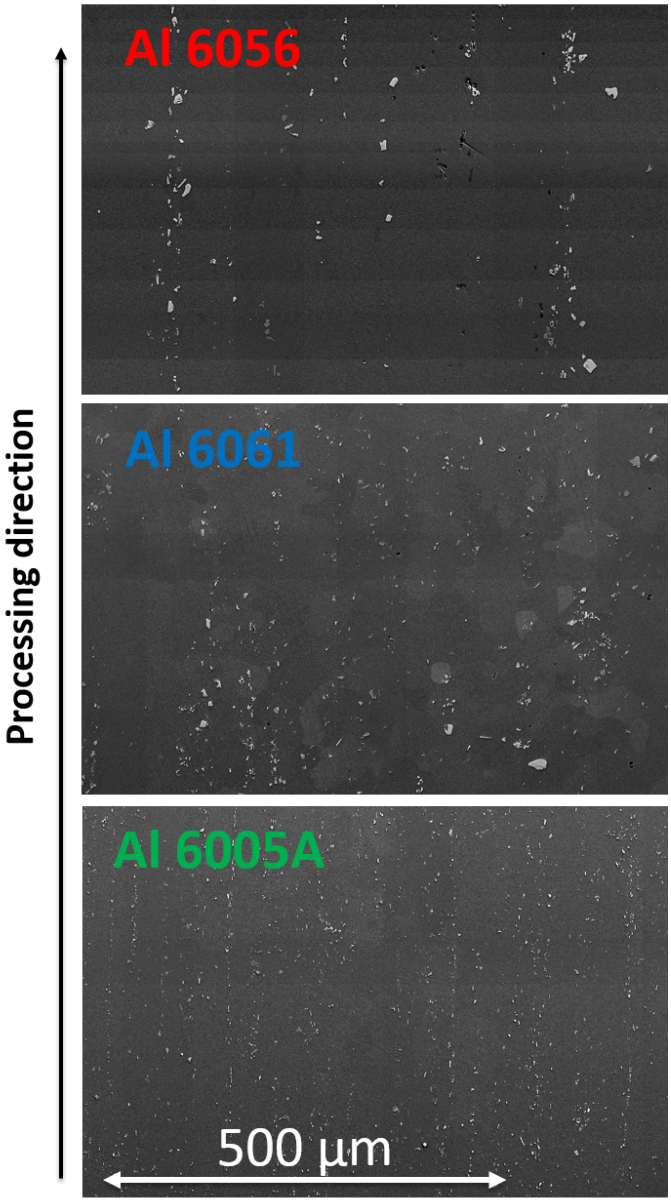

Figure 2: SEM micrographs taken in the processing-transverse plane showing the distribution of intermetallic particles (in white) in the alloys Al 6056, Al 6061 and Al 6005A.

representative of the microstructure as it encompasses the effect of the particles size, shape, orientation and spatial distribution. The two-point correlation function, which is closely related to the PCF described here, has been largely discussed in <28; 29; 30> and already been used to characterize anisotropic microstruc-

tures <31>. The PCF has already been successfully used to quantify for instance the effect of 3D particles distributions on particle stimulated nucleation during recrystallization <32> or to quantify microstructure homogeneization by friction stir processing <10>.

The PCF analysis is directly applied in 2D to the SEM images and in 3D to the microtomography images. In the 3D case, 2D cuts of the PCF in the processing-transverse plane are plotted in order to allow direct comparison with the analysis performed in 2D on SEM images. The PCF of the Al 6056, Al 6061 and Al 6005A are shown in Fig. 3. Globally, Fig. 3 shows that the SEM and microtomography based PCF are similar for all three alloys. Clearly, the PCF is anisotropic in each case with the highest PCF value parallel to the processing direction. As already explained, this is due to the stringer-type clustering along the processing direction. The anisotropy of the PCF of the Al 6056 (Fig. 3(a)) is very pronounced, with high PCF values (≈ 4) along the rolling direction, extending over the entire frame (more than 50 μm). On the opposite, the anisotropy observed in the PCF corresponding to the alloys Al 6061 and Al 6005A is less marked. Indeed, the area with high PCF values is more confined in both cases compared to the Al 6056. If a PCF value larger than 3 is chosen as an indicator of particle clustering, the analysis indicates that particles are clustered into long bands in the Al 6056. On the opposite, particles are arranged into stringer-type clusters extending over a length of ≈ 25 μm for the Al 6061 and ≈ 10 μm for the Al 6005A.

3.2.2. Quantification of particle clustering

In the previous section, it was shown with the PCF analysis that the anisotropic ductility of the Al 6056 is caused by a very pronounced anisotropy of the particle distribution, while it is less marked in the alloys Al 6061 and Al 6005A. However, this conclusion is based on cross-comparison only and an inherent problem of the PCF analysis is that it does not provide an absolute criterion that would indicate if the degree of anisotropy of the clustering is large enough to affect the macroscopic ductility. This is due to the fact that the PCF analysis does not distinguish between the contribution from particles belonging to the same cluster and particles belonging to different clusters, i.e. the PCF does not provide information about the percolation of clusters <28>.

An analysis proposed by Achon et al. <33> was used to further characterize the clusters within the 2D particle field observed by SEM. This procedure distinguishes isolated particles, i.e. particles that are dis-

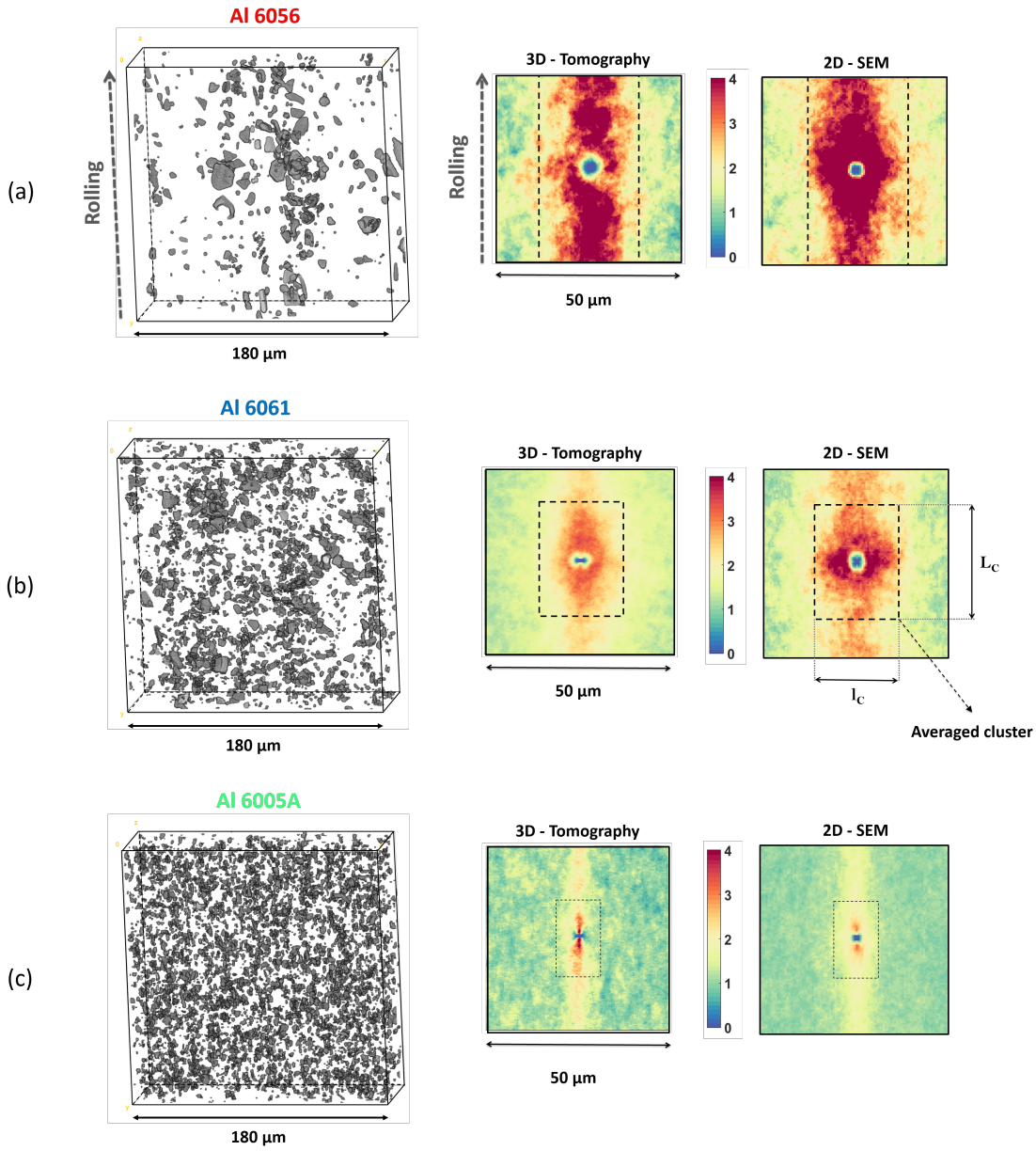

Figure 3: (*Left*) 3D microtomography perspective of particles distribution in the aluminium alloys (*a*) 6056, (*b*) 6061 and (*c*) 6005A and (*Right*) corresponding pair correlation functions (PCFs) for the RD-TD plane through the center of the sub-volume. A PCF value smaller or larger than one corresponds respectively to a smaller or larger probability to find a neighbor in the vicinity of a particle compared to a perfectly homogenous distribution.

tant from all their neighbours by a distance (from centroid to centroid) larger than a distance defined thus

as $d_{Cluster}$, from particles belonging to clusters. The distance $d_{Cluster}$ is an objective (i.e. user independent) characteristic of the particles spatial distribution. When the distance $d_{Cluster}$ increases, the number of clusters increases. At some point, the number of identified clusters starts to decrease because the distance $d_{Cluster}$ becomes so large that the clusters coalesce with one another. The clustering distance of the distribution selected here is the value of $d_{Cluster}$ corresponding to the maximum number of clusters identified within the particle field, see <22> for more details on Achon's method. A visualisation of a few clusters is shown if Fig. 4 for the three alloys. White particles correspond to isolated particles and particles with the same color belong to the same cluster.

The main indicators resulting from the clustering analysis are shown in Table 1. The characteristic clustering distance $d_{Cluster}$ decreases with the size of the particles (equal to 1.3μm, 2.1μm, and 3.1μm for the Al 6005A, Al 6061 and Al 6056, respectively). Indeed, since the volume fraction of particles is approximately the same in the three alloys, the number of particles per unit volume increases (the average distance between particles decreases) when the particles size decreases. However, the average number of particles forming a cluster is always about 9 and the percentage of particles which are located inside clusters is always approximately 60%. The size and the shape of the clusters have been characterized with the minimum bounding box enclosing all the particles belonging to the same cluster. The average side length of the box along the rolling/extrusion direction is given by L_C and the side length along the transverse direction is given by l_C. The averaged bounding box of the clusters in Table 1 has been reported for each alloy in Fig. 3. The clustering analysis is coherent with the PCF analysis in terms of cluster size and shape. Indeed, in each case, the average cluster approximately corresponds to the zone which contains all PCF values larger than 3. A threshold value of 3 will thus be used in the following in order to identify particle clustering from PCF analysis.

Parameter	**Al 6056**	**Al 6061**	**Al 6005A**
Clustering distance $d_{Cluster}$	22.5 μm	13.5 μm	7.5 μm
Average number of particles forming a cluster	9.3 particles	9.6 particles	8.5 particles
% of particles within clusters (volume-weighted)	62.3 %	63.8 %	63.4 %
Cluster size (L_c/l_c)	57/27 μm	31/23 μm	21/12 μm

Table 1: Indicators resulting from the clustering analysis.

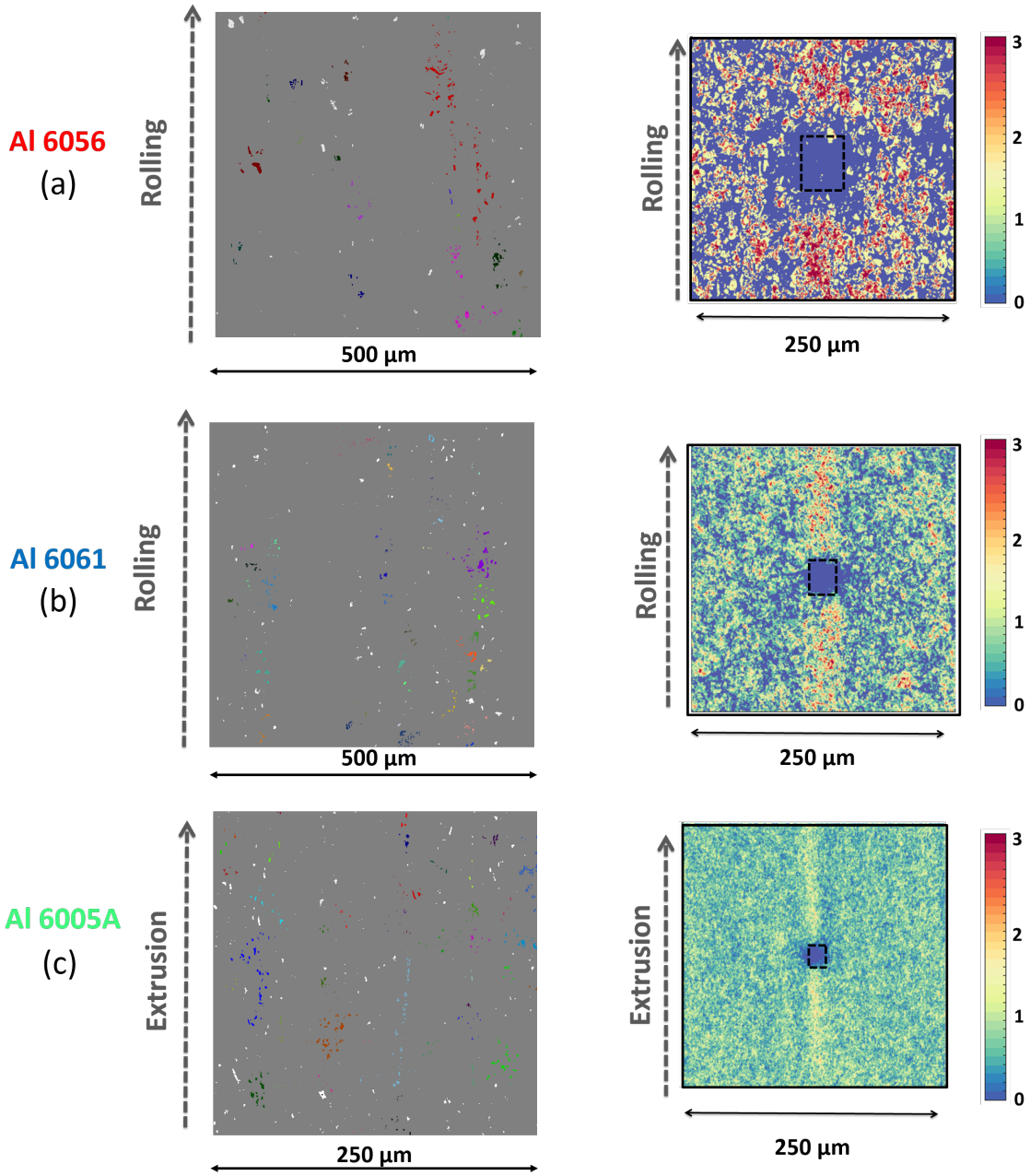

Figure 4: (*Left*) Visualisation of a few clusters from particle distribution shown in the SEM images of Fig. 2. (*Right*) PCF analysis performed on clusters from SEM images for the alloys (*a*) Al 6056, (*b*) Al 6061 and (*c*) Al 6005A.

3.2.3. Quantification of the clustering anisotropy

After the identification of the clusters, the cluster distribution itself can be characterized by the PCF analysis as well. Thus, each cluster is treated as a group and the PCF analysis is performed in the same way as previously but, this time, on clusters. The large particle fields characterized by SEM contain several hundreds of clusters allowing a statistical analysis of their arrangement. The results are shown in Fig. 4. The central box represents the average cluster size characterized with the minimum bounding box enclosing all the particles belonging to the same cluster, as already explained in section. 3.2.2. This average cluster size is larger for Al 6056 compared to Al 6061 and Al 6005A. Large scale clustering approximately corresponds to the zone which contains all PCF values higher than about 3. In the Al 6056 (Fig. 4(a)), large-scale clustering appears along the rolling direction. In other words, there is a large-scale clustering (i.e. clusters of clusters) along the rolling direction. On the opposite, in the Al 6061 and Al 6005A (Fig. 4(b,c)), the PCF analysis is much more homogeneous. The anisotropy of the PCF remains very limited and the PCF is close to 1 everywhere, with no large-scale clustering.

The analysis indicates that the anisotropy of the ductility in the Al 6056 is linked to the length scale over which the particle distribution exhibits anisotropy, and this will be further clarified in the following section.

3.3. Damage evolution: experimental results

Figure 5 shows a 2D cut through the middle of two tensile specimens, just before fracture, loaded either along the transverse (Fig. 5(a)) or the rolling direction (Fig. 5(b)). The evolution of the minimum cross-sectional area in the necking region (A_{loc}) provides an estimate of the local true tensile strain $\varepsilon_{loc}=\ln\left(\frac{A_0}{A_{loc}}\right)$ and of the true macroscopic axial stress $\sigma_{zz} = F/A_{loc}$. The tensile stress-strain curves extracted from the in situ data is given in Fig. 5(c) for both loading directions up to large deformations. Figure 5(c) shows that plastic anisotropy is small as already concluded from the macroscopic tensile tests. The influence of the spatial distribution of intermetallic particles can be quantitatively observed in the insets of Fig. 5(a) and Fig. 5(b). When loading in the transverse direction, coalescence events are already detected at the early stages of necking. Looking at the inset of Fig. 5(a), coalescence events are generalized inside clusters (i.e. intracluster coalescence) at deformation levels similar to the uniform elongation (i.e. well before fully developed necking). On the contrary, when the loading is in the rolling direction (see the inset of Fig. 5(b)), a stable void growth process is pursued even after significant amount of necking, with only a very small

number of coalescence events.

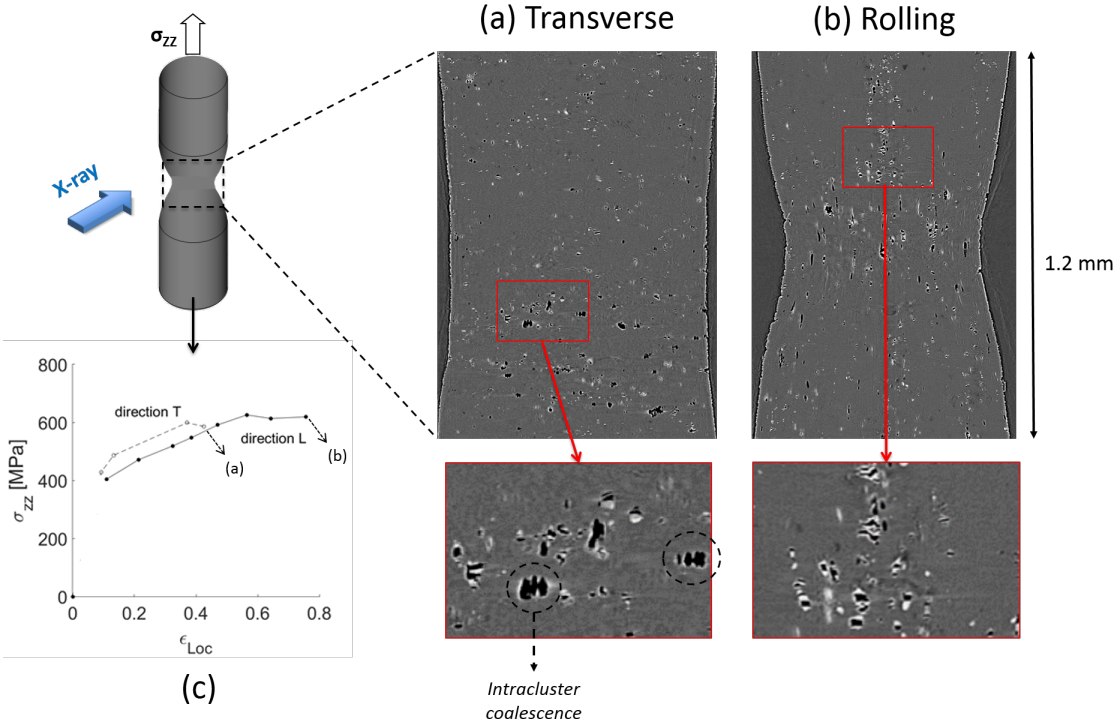

Figure 5: X-ray microtomography reconstructed images just before fracture, of the tensile test performed on the alloy Al 6056-T4 loaded in (*a*) the transverse direction and (*b*) the rolling direction. Voids appear in black in the grey matrix and IM particles appear in white. The tensile curves in (*c*) correspond to the in situ tensile tests shown in (*a*) and (*b*).

There exist thus two coalescence stages of ductile damage within heterogeneous materials that include intra- and inter-cluster coalescence <15; 34>. The evolution of damage is thus strongly influenced by the degree of anisotropy of the particle clusters. The sequence is analyzed in more details in the following paragraphs.

a) Intra-cluster coalescence. Early intra-cluster coalescence stage is observed in the in situ testing scans of the Al 6056 along the rolling direction, see Fig. 6(*a*) and (*b*) in which a few clusters involving some coalescence events have been encircled. Intra-cluster coalescence consists in the linking of a few voids over a distance of approximately 50 μm, in good agreement with the cluster size (see Fig. 3(*a*) and Table 1).

b) Inter-cluster coalescence. The final fracture is triggered by a second stage of inter-cluster coales-

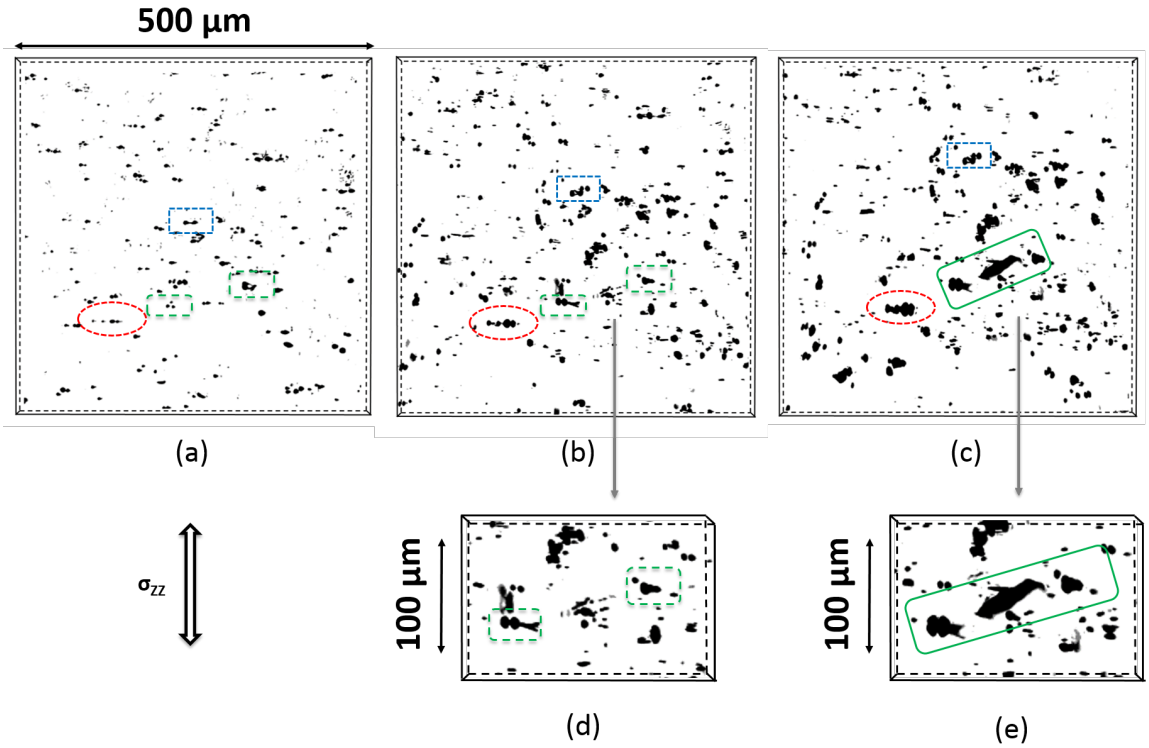

Figure 6: Void distribution observed during in-situ microtomography in the alloy Al 6056 loaded in the transverse direction at a local strain of (*a*) ϵ_{Loc} = 0.1, (*b*) ϵ_{Loc} = 0.35 and (*c*) ϵ_{Loc} = 0.43. (*d*) Zoom of figure (*b*), showing the formation of a second population of voids between two clusters of voids. (*e*) Zoom of figure (*c*), showing the intercluster coalescence with the formation of micro shear band.

cence which leads to the collapse of the matrix ligament between microcracks formed by the intra-cluster coalescence stage. Again, this is in good agreement with what is observed in Fig. 6(*c*) which corresponds to the material state just before fracture. This shear localization between clusters should not be confused with a macroscopic shear localization extending over many voids at a larger scale <35>. Indeed, the cluster localization is occurring at a mesoscale, over a distance of approximately 150μm.

c) Coalescence mechanisms at the different length scales. Figure 6(*d*) shows a zoom of two microcracks formed by intra-cluster coalescence, which confirmed the internal necking process. The formation of a second population of cavities is also observed in the ligament between these two microcracks. Figure 6(*e*) shows a zoom of the two same microcracks at a slightly larger deformation. The ligament between these microcracks is collapsing by void sheeting initiated on this second population of cavities. These experimen-

tal observations are in good agreement with the modeling results from literature, as detailed in the following section.

4. Discussion on the origins of the failure anisotropy

First, early coalescence events mainly occur inside particle clusters. Thomson *et al* <15> have shown that coalescence of voids within a cluster, i.e. intra-cluster or void-to-void coalescence, is a stable event which does not directly lead to material failure but is followed by a second void growth process based on these early coalesced microcracks. Figure 7 schematically rationalizes the void interactions occurring inside a cluster of particles. The cracking of an intermetallic particle changes the strain field in the surrounding matrix and creates a region of elevated strain in the close neighbourhood, see Fig. 7. The process of void coalescence is favoured when the loading is in the transverse direction due to enhanced interaction of the strain fields surrounding closely spaced voids (see Fig. 7(*a*)) facilitating the localization of plasticity in the intervoid ligament. On the contrary, when the loading is in the rolling direction, there is less interaction of the local strain fields associated to the voids due to their spatial distribution (see Fig. 7(*b*)).

The final fracture is triggered by inter-cluster coalescence which is favoured when the loading is in the transverse direction because clusters are closer to one another (see Fig. 7(*c*) and (*d*)). Furthermore, this second coalescence stage is likely to occur much faster in the case of an anisotropic large-scale clustering, i.e. linear clusters forming almost continuous elongated bands (see Fig. 7(*c*)). On the opposite, the effect of particle clustering on the second stage of void coalescence will be weak in case of a more homegenous distribution of clusters (see Fig. 7(*d*)), because their interaction is weaker.

According to the unit cell model of Thomson<15>, intra-cluster coalescence occurs by internal necking of the intervoid ligament. In contrast, the second coalescence stage between distant microcracks occurs through void-sheeting, i.e. internal shearing of the ligament, and this is favoured by the nucleation of a secondary void population. Bandstra *et al*. <36> also observed a void-sheet failure mechanism at high triaxiality in a HY-100 steel plate. The void-sheet coalescence mechanism was explained by a strong tendency for intense strain localization between stringers of inclusions despite their large spacing. According to this study, the nucleation of a secondary void population between the primary voids enhances (but does not cause) the plastic strain localization that results in void-sheet coalescence. This is in good agreement with

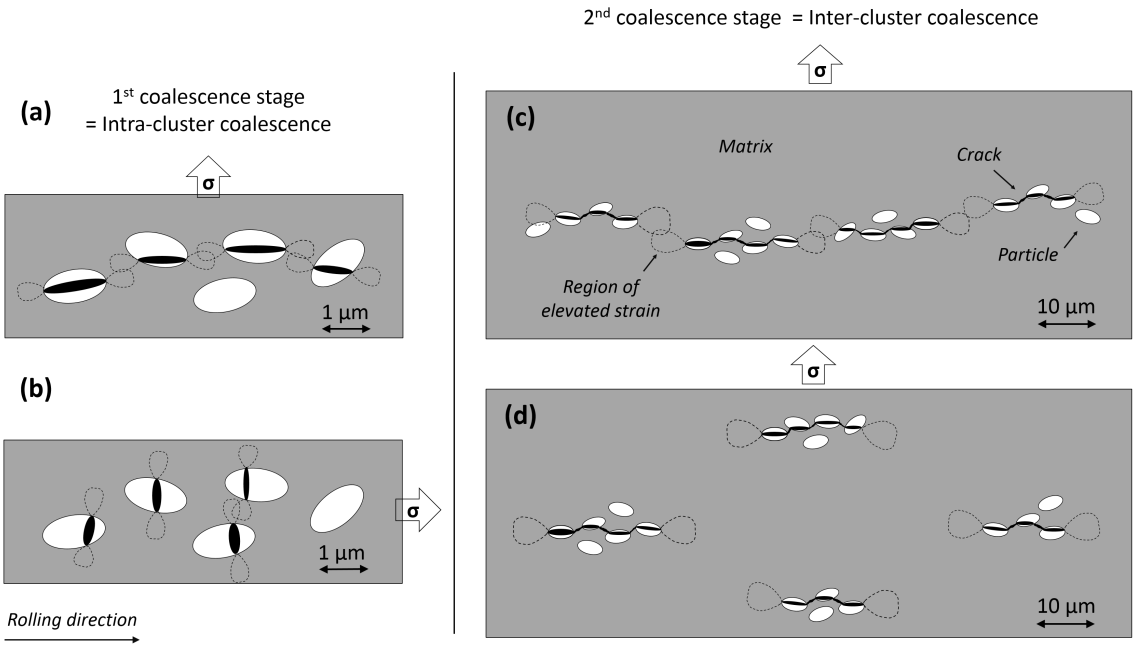

Figure 7: Schematic of the effect of microstructural anisotropy on the damage percolation process. The effect of the stringer orientation on the first coalescence stage (i.e. intra-cluster) is shown in (*a*) and (*b*). The effect of the clusters distribution on the second coalescence stage (i.e. inter-cluster) is shown in (*c*) and (*d*). In the case of discontinuous stringer (*d*), a second void growth process based on the early coalesced voids sets in until second coalescence.

what has been observed in Fig. 6.

The anisotropy of ductility observed in the alloy Al 6056 is closely related to stringer-type particle clustering along the rolling direction. However, this type of anisotropic microstructure is also found in the alloy Al 6061 and the alloy Al 6005A for which the fracture strain is close to isotropic (see section. 3.2.1). The results of section 3.2.3 indicate that the dependence of the ductility on the loading direction in the alloy Al 6056 is linked to the length scale over which the particle distribution exhibits a strong degree of anisotropy. Indeed, the alloy Al 6056 exhibits a strong anisotropic large-scale clustering of particles, i.e. particle clusters are much closer to each other in the rolling direction compared to the transverse direction. This is schematically represented in Fig. 8.(*a*). This proximity of clusters creates an easy percolating crack path along the rolling direction as a crack can extend along this direction throughout the material without the need to cross a tougher matrix material (presenting much less damage), see Fig. 8(*b*) and (*c*).

On the opposite, particle stringers are more isolated in the case of the alloys Al 6061 and Al 6005A (see

Fig. 8(*d*)). The presence of a tougher matrix between these clusters strongly reduces the detrimental effect of the clusters and the anisotropy of fracture properties by allowing a second stage of stable void growth between clusters (see Fig. 8(*e*) and (*f*)). It is thus the degree of continuity of the particle stringers over significant distances, i.e. large-scale clustering, which sets the fracture anisotropy of the alloy Al 6056.

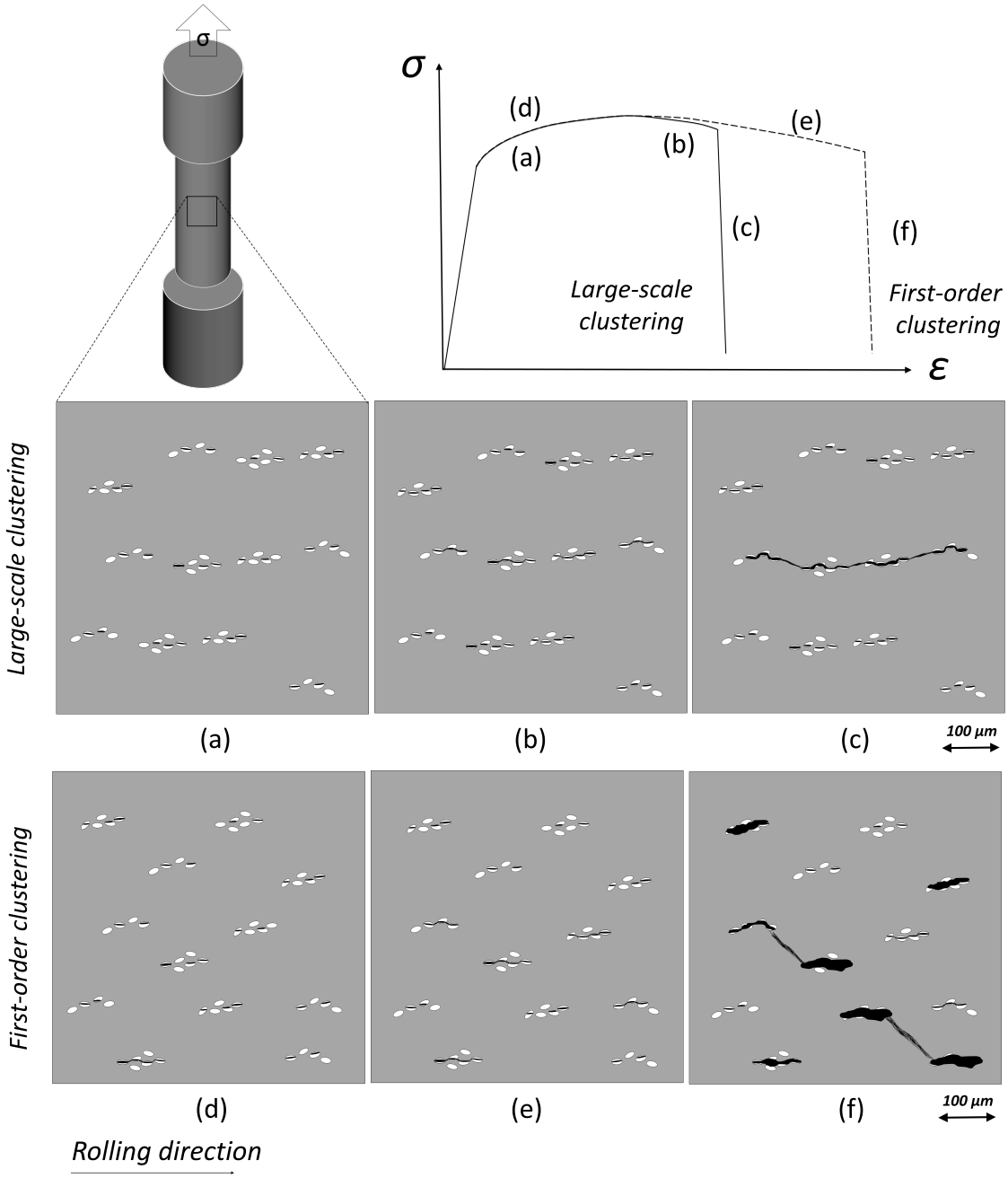

Figure 8: Schematics of the damage sequence in the alloy Al 6056 ((*a*), (*b*) and (*c*)), and in the alloys Al 6061 and 6005A ((*d*), (*e*) and (*f*)).

5. Conclusion

The hardening and fracture properties of three aluminium alloys of the 6xxx series have been determined for different heat treatment conditions and for two different loading directions. The key results of the study are the following:

- The macroscopic tensile tests indicate that the yielding and hardening behaviour is almost isotropic for the three alloys. The fracture strain is significantly larger in the rolling direction compared to the transverse direction in the alloy Al 6056, but not in the alloys Al 6061 and Al 6005A for which ductility is almost isotropic.

- In situ tensile tests during X-ray tomography have confirmed the existence of two coalescence stages of ductile damage which consist of intra- and inter-cluster coalescence.

- The Pair Correlation Function (PCF) is used to quantify the effect of the particle spatial distribution on damage. The PCF analysis has been performed both on the 3D tomography data and on SEM images, leading to very similar results.

- The PCF is shown to be an effective way to quantify the degree of first-order and large-scale clustering within a particle field, and to identify the preferred orientation of these clusters, if any. It also allows the comparison of the relative amount of clustering between different particle fields.

- The analysis indicates that it is the degree of continuity of the particle stringers over distances comparable to macroscale, i.e. large-scale clustering, which sets the magnitude of the fracture anisotropy. If particle clusters appear under the shape of continuous elongated bands, the ductility of the material is likely to exhibit a significant anisotropy. In the case of shorter and isolated particle stringers, the presence of tougher matrix between these clusters strongly reduces the anisotropy of fracture properties by allowing a second stage of stable void growth at the scale of the clusters. The alloy Al 6056 presents continuous elongated bands at the mesoscale explaining its failure anisotropy.

This study illustrates how the PCF can be used to quantify the effect of microstructural anisotropy on macroscopic fracture properties. The results demonstrate the strong influence of mesoscale heterogeneities on the damage evolution in case of heterogeneous material. Nowadays, damage models implemented in FE software are still usually limited to isotropic behaviour. This work emphasizes the need for better representation of the microstructure heterogeneities, such as clustering and microstructure anisotropy. The studied

alloys do not exhibit significant anisotropy of yielding which allowed isolating the effect of the particle distribution on the anisotropy of damage properties. However, in many cases, the anisotropy comes from both contributions. In this case, the PCF analysis could be used as a first step for evaluating the degree of anisotropy which is expected for a specific microstructure and for producing statistically representative particle fields. Furthermore, the quantification of the anisotropy of the microstructure plays a key role in manufacturing. For example, the alloy 6005A has been extruded and this could maybe explain why the clustering is the least pronounced in this alloy. Finally, the PCF analysis is not limited to the question of damage propagation as there are many physical properties which depend on the homogeneity of the microstructure. For example, clusters of particles have been shown to form the most severe corrosion pits <37> and to strongly impact the nucleation of recrystallization <32>. Another example is the role of fibre clusters in the problem of internal stresses in composites related to the difference in thermal expansion during processing <38>.

Acknowledgments

The authors would like to thank SLS for the attribution of beamtime on the TOMCAT beamline and Anne Bonnin for her help as local contact. F. Hannard acknowledges the financial support of the FRIA, Belgium.

References

[1] A. Pineau and T. Pardoen. Failure of metals. In *Compr. Struct. Integr. 2*, pages 684 – 797. 2007.

[2] A. L. Gurson. Continuum theory of ductile rupture by void nucleation and growth, 1. Yield criteria and flow rules for porous ductile media. *J. Eng. Mater. Technol.*, 99(1):2 – 15, 1977.

[3] V. Tvergaard and A. Needleman. Analysis of the cup-cone fracture in a round tensile bar. *Acta Metall.*, 32(1):157 – 169, 1984.

[4] T. Pardoen and J. W. Hutchinson. An extended model for void growth and coalescence. *J. Mech. Phys. Solids*, 48(12):2467 – 2512, 2000.

[5] A.A. Benzerga and J. Besson. Plastic potentials for anisotropic porous solids. *Eur. J. Mech. A. Solids*, 20(3):397 – 434, 2001.

[6] A. Pineau, A.A. Benzerga, and T. Pardoen. Failure of metals i: Brittle and ductile fracture. *Acta Mater.*, 107:424 – 483, 2016.

[7] M. Brunet, F. Morestin, and H. Walter. Damage identification for anisotropic sheet-metals using a non-local damage model. *Int. J. Damage Mech.*, 13(1):35–57, 2004.

[8] A.A. Benzerga and J.B. Leblond. Ductile fracture by void growth to coalescence. In *Adv. Appl. Mech.*, volume 44, pages 169 – 305. 2010.

[9] H. Agarwal, A. M. Gokhale, S. Graham, and M. F. Horstemeyer. Anisotropy of intermetallic particle cracking damage evolution in an al-mg-si base wrought aluminum alloy under uniaxial compression. *Metall. Mater. Trans. A*, 33(11):3443 – 3448, 2002.

[10] F. Hannard, S. Castin, E. Maire, R. Mokso, T. Pardoen, and A. Simar. Ductilization of aluminium alloy 6056 by friction stir processing. *Acta Mater.*, 130:121 – 136, 2017.

[11] F. Beremin. Cavity formation from inclusions in ductile fracture of a508 steel. *Metall. Mater. Trans. A*, 12:723–731, 1981.

[12] S.M. Keralavarma and A.A. Benzerga. A constitutive model for plastically anisotropic solids with non-spherical voids. *J. Mech. Phys. Solids*, 58(6):874 – 901, 2010.

[13] J. Koplik and A. Needleman. Void growth and coalescence in porous plastic solids. *Int. J. Solids Struct.*, 24(8):835 – 853, 1988.

[14] D. Lassance, F. Scheyvaerts, and T. Pardoen. Growth and coalescence of penny-shaped voids in metallic alloys. *Eng. Fract. Mech.*, 73(8):1009 – 1034, 2006.

[15] C.I.A. Thomson, M.J. Worswick, A.K Pilkey, and D.J. Lloyd. Void coalescence within periodic clusters of particles. *J. Mech. Phys. Solids*, 51(1):127 – 146, 2003.

[16] A.K. Pilkey, M.J. Worswick, C. I. E. Thomson, G. Burger, and D.J. Lloyd. Effect of second-phase particle clustering on formability of al-si sheet. *Alpas, A. (Eds.), Advances in Industrial Materials. Canadian Institute of Mining, Metallurgy and Petroleum, Montreal.*, 2008.

[17] D. Steglich, W. Brocks, J. Heerens, and T. Pardoen. Anisotropic ductile fracture of al 2024 alloys. *Eng. Fract. Mech.*, 75(12):3692 – 3706, 2008.

[18] M.J. Worswick, Z.T. Chen, A.K. Pilkey, D. Lloyd, and S. Court. Damage characterization and damage percolation modelling in aluminum alloy sheet. *Acta Mater.*, 49(14):2791 – 2803, 2001.

[19] P.O. Bouchard, L. Bourgeon, H. Lachaple, E. Maire, C. Verdu, R. Forestier, and R.E. Loge. On the influence of particle distribution and reverse loading on damage mechanisms of ductile steels. *Mater. Sci. Eng. A*, 496(1):223 – 233, 2008.

[20] T. Pardoen and J. W. Hutchinson. Micromechanics-based model for trends in toughness of ductile metals. *Acta Mater.*, 51(1):133 – 148, 2003.

[21] A. A. Benzerga, J. Besson, and A. Pineau. Anisotropic ductile fracture: Part i : experiments. *Acta Mater.*, 52(15):4623 – 4638, 2004.

[22] F. Hannard, T. Pardoen, E. Maire, C. Le Bourlot, R. Mokso, and A. Simar. Characterization and micromechanical modelling of microstructural heterogeneity effects on ductile fracture of 6xxx aluminium alloys. *Acta Mater.*, 103:558 – 572, 2016.

[23] M.Stampanoni, F. Marone, P. Modregger, B. Pinzer, T. Thuring, J. Vila Comamala, C. David, and R. Mokso. Tomographic hard xray phase contrast micro and nano imaging at tomcat. *AIP Conference Proceedings*, 1266(1):13–17, 2010.

[24] J.-Y Buffière, E. Maire, P. Cloetens, G. Lormand, and R. Fougères. Characterization of internal damage in a mmcp using x-ray synchrotron phase contrast microtomography. *Acta Mater.*, 47(5):1613 – 1625, 1999.

[25] E. Maire, O. Bouaziz, M. Di Michiel, and C. Verdu. Initiation and growth of damage in a dual-phase steel observed by x-ray microtomography. *Acta Mater.*, 56(18):4954 – 4964, 2008.

[26] Y. Chen, A.H. Clausen, O.S. Hopperstad, and M. Langseth. Stressstrain behaviour of aluminium alloys at a wide range of strain rates. *Int. J. Solids Struct.*, 46(21):3825 – 3835, 2009.

[27] A. D. Rollett, S.B. Lee, and R. Campman. Three-dimensional characterization of microstructure by electron back-scatter diffraction. *Annual Reviews*, 2007.

[28] S. Torquato. *Random Heterogeneous Materials: Microstructure and Macroscopic Properties*. Interdisciplinary Applied Mathematics. Springer New York, 2005.

[29] S. Ghosh and D. Dimiduk. *Computational Methods for Microstructure-Property Relationships*. Springer US, 2010.

[30] S.R. Kalidindi. *Hierarchical Materials Informatics: Novel Analytics for Materials Data*. Elsevier Science, 2015.

[31] A.M. Gokhale, A. Tewari, and H. Garmestani. Constraints on microstructural two-point correlation functions. *Scripta Mater.*, 53(8):989 – 993, 2005.

[32] K. Marthinsen, J.M. Fridy, T.N. Rouns, K.B. Lippert, and E. Nes. Characterization of 3-d particle distributions and effects on recrystallization kinetics and microstructure. *Scripta Mater.*, 39(9):1177 – 1183, 1998.

[33] Ph. Achon. *Comportement et tenacite d'alliages d'aluminium a haute resistance*. PhD thesis, Ecole nationale superieure des mines (Paris), 1994.

[34] O.S. Orlov, M.J. Worswick, E. Maire, and D.J. Lloyd. Simulation of damage percolation within aluminum alloy sheet. *J. Eng. Mater. Techn.*, 131(2):021001, 2009.

[35] C. Tekoğlu, J.W. Hutchinson, and T. Pardoen. On localization and void coalescence as a precursor to ductile fracture. *Philo. Trans. R. Soc. London, Ser. A*, 373(2038), 2015.

[36] J.P Bandstra and D.A Koss. Modeling the ductile fracture process of void coalescence by void-sheet formation. *Mater. Sci. Eng. A*, 319:490 – 495, 2001.

[37] M.J. Cullin, D.G. Harlow, and R.P. Wei. Modeling and simulation of constituent particle clustering and distribution in rolled aluminum alloys. *Model. Simul. Mater. Sci. Eng.*, 19(3):035004, 2011.

[38] Y. J.M. Brechet. Clusters, plasticity and damage: a missing link? *Mater. Sci. Eng. A*, 175(1):63 – 69, 1994.